Posture stabilization of a unicycle mobile robot – two control approaches

Krzysztof Kozłowski, Jarosław Majchrzak, Maciej Michałek, Dariusz Pazderski*

1 Introduction

State feedback control issues for nonholonomic systems are still very challenging for control researchers. Among the group of nonholonomic systems one can number wheeled mobile vehicles, manipulators with nonholonomic gears, free-floating robots, underwater vessels, nonholonomic manipulator's grippers, dynamically balanced hopping robots and others [10], [15], [4]. Difficulties in designing effective stabilizers arise from nonintegrable kinematic constraints imposed on system evolution. These constraints impose restriction on admissible velocities of controlled dynamic systems, preserving however their controllability. Moreover, lower dimensionality of the control space $U \subset \mathbb{R}^m$ in comparison to configuration space $\mathcal{Q} \subset \mathbb{R}^n$ $(n > m)$ causes difficulties in control design, especially for stabilization task problem [5]. Despite mentioned problems, many different feedback control strategies for nonholonomic kinematics in automatics and robotics literature have been proposed – see for example [7], [18] or [8]. Although some important problems, like robustness to control signals limitations existance, intuitive contoller parameters tunning and good control quality during transient stage seem to be still open issues and involve further research. In this paper two different stabilization approaches, which regard mentioned problems with alternative solution in comparison with existing strategies, will be described. Presented approaches will be applied to derive two stabilizers to solve the stabilization task for a unicycle mobile robot, taking into account control limitations. The first controller, which may be classified as Time-Varying Oscillatory (TVO) stabilizer, is based on an idea of stabilization initially proposed by Dixon *et al.* and next generalized by Morin and Samson [17]. The second approach results from a novel concept called the Vector Field Orientation (VFO) approach introduced for the first time in [12]. For both stabilizers, control signal limitations will be considered at the kinematic level as restrictions imposed on a maximal velocity of robot wheels. Effectiveness of the proposed control strategies will be compared and illustrated by simulation results.

2 Kinematics

This work considers a unicycle mobile robot, which can be treated as a reduced two-wheeled differentially driven mobile vehicle with angular, Ω, and linear, V, velocities chosen as input controls. Assuming nonexistence of lateral slippage of robot wheels,

*Chair of Control and Systems Engineering, Poznań University of Technology (PUT), Piotrowo 3a, 60-965 Poznań, Poland, e-mail: {name.surname}@put.poznan.pl

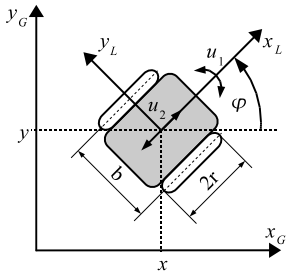

Figure 1: Mobile robot in the global frame $\{G\}$.

kinematic model of a unicycle mobile robot can be described in the following manner:

$$\begin{bmatrix} \dot{\varphi} \\ \dot{x} \\ \dot{y} \end{bmatrix} = \begin{bmatrix} 1 \\ 0 \\ 0 \end{bmatrix} u_1 + \begin{bmatrix} 0 \\ \cos\varphi \\ \sin\varphi \end{bmatrix} u_2, \tag{1}$$

where $\boldsymbol{q} \triangleq [\varphi\ x\ y]^T \in \mathcal{Q} \subset \mathbb{R}^3$ denotes the state vector and $u_1 = \Omega, u_2 = V \in \mathbb{R}$ describe control inputs (see Fig. 1). Model (1) belongs to a class of underactuated nonholonomic driftless systems with two inputs described in the following general form:

$$\dot{\boldsymbol{q}} = \boldsymbol{g}_1 u_1 + \boldsymbol{g}_2(\boldsymbol{q}) u_2, \tag{2}$$

where $\boldsymbol{g}_1, \boldsymbol{g}_2(\boldsymbol{q})$ are basic vector fields – generators. From the last two equations of (1) one can derive the assumed nonitegrable velocity constraint:

$$\boldsymbol{A}(\boldsymbol{q})\dot{\boldsymbol{q}} = 0, \qquad \boldsymbol{A}(\boldsymbol{q}) = [0\ \sin\varphi\ -\cos\varphi], \tag{3}$$

where $\dot{\boldsymbol{q}} \triangleq [\dot{\varphi}\ \dot{x}\ \dot{y}]^T \in \mathbb{R}^3$ is the generalized state velocity and $\boldsymbol{A}$ is called the constraint matrix. It is well known, that the system (1) is fully controllable in $\mathcal{Q}$, however all generalized state velocities $\dot{\boldsymbol{q}}$ accessible during time evolution exclude some set of instantaneously inadmissible movement directions. This constraint together with less number of inputs in relation to the state vector dimension cause difficulties in solving control tasks, especially for the point stabilization task [5].

3 Posture stabilization - two control approaches

In this paper posture stabilization in Cartesian space of the system (1) is considered. In order to determine posture error the following vector $\boldsymbol{e}(\tau) \in \mathbb{R}^3$ is defined

$$\boldsymbol{e}(\tau) \triangleq \begin{bmatrix} e_1(\tau) \\ e_2(\tau) \\ e_3(\tau) \end{bmatrix} \triangleq \boldsymbol{q}_t - \boldsymbol{q}(\tau) = \begin{bmatrix} \varphi_t - \varphi(\tau) \\ x_t - x(\tau) \\ y_t - y(\tau) \end{bmatrix}, \tag{4}$$

where $\boldsymbol{q}_t$ and $\boldsymbol{q}(\tau)$ determine the reference (desired) and actual state vectors, respectively, and the time variable has been denoted by τ.

In the sequel two alternative control approaches, which allow to solve practical or asymptotic posture stabilization for nonholonomic kinematics (1) will be described.

The control task considered in this paper, called hereafter as a *stabilization task*, can be defined as follows.

Definition 1 (Stabilization task) *Find bounded controls $u_1(\tau), u_2(\tau)$ for kinematics (1) such, that for initial condition $\boldsymbol{e}(0) \in \mathcal{E} \subset \mathbb{R}^3$ the Euclidean norm of the error $\boldsymbol{e}(\tau)$ tends to some constant $\varepsilon > 0$ as $\tau \to \infty$:*

$$\lim_{\tau \to \infty} \|\boldsymbol{e}(\tau)\| = \varepsilon, \tag{5}$$

where ε is an assumed error envelope, which can be made arbitrary small. For $\varepsilon > 0$ above statement defines practical stabilization task, and for $\varepsilon = 0$ – asymptotic convergence task.

3.1 Oscillatory-based time-varying control law

The first control method (TVO) is based on tuned oscillator idea introduced by Dixon *et al.* [9]. It should be noted that this approach can be seen as a particular case of more general theory developed by Morin and Samson [17], taking advantage of so-called transverse functions. The main feature concerning these control schemes lies in virtual periodic signals tracked by the state vector of the system.

3.1.1 Model transformation

In control theory area much works were devoted to the stabilization problem of the abstract mathematical objects which are not related to the physical systems directly. Such approach allows for generalization of control solutions applicable to some class of systems which are, in general, much simpler than original ones. In particular, so-called chained canonical form, were investigated during the last fifteen years. As it was pointed out by many authors (see for example [14, 22, 17]) mathematical models used to describe different physical systems which includes, for example, kinematics of the most terrain vehicles, may be transformed to the chained form using properly chosen transformation.

In this section we present a control law taking advantage of mathematical properties of the system known as Brockett's nonholonomic integrator [6]. This is the driftless nilpotent system for which controllability in a short time is ensured by the first order Lie bracket. The nonholonomic integrator can be written in the following form (compare [9])

$$\dot{\boldsymbol{x}}^* = \boldsymbol{v}, \tag{6}$$

$$\dot{x}_3 = \boldsymbol{x}^{*T} \boldsymbol{J} \boldsymbol{v}, \tag{7}$$

where $\boldsymbol{x} = \begin{bmatrix} x_1 & x_2 & x_3 \end{bmatrix}^T = \begin{bmatrix} \boldsymbol{x}^{*T} & x_3 \end{bmatrix}^T \in \mathbb{R}^3$ is a state vector, $\boldsymbol{v} = \begin{bmatrix} v_1 & v_2 \end{bmatrix}^T \in \mathbb{R}^2$ denotes an input and $\boldsymbol{J} = \begin{bmatrix} 0 & -1 \\ 1 & 0 \end{bmatrix}$ is the skew-symmetric matrix.

In order to transform kinematic equation (4) to the form of nonholonomic integrator the following nonlinear transformation considered by Dixon et al. [9] may be used (for derivation of the transformation see [20])

$$\boldsymbol{x} \triangleq -\boldsymbol{P}(\boldsymbol{q}, \boldsymbol{e})\, \boldsymbol{e}, \tag{8}$$

where $\boldsymbol{P}$ defines global diffeomorphism with respect to the origin

$$\boldsymbol{P}\left(\theta, \tilde{\theta}\right) \triangleq \begin{bmatrix} 1 & 0 & 0 \\ 0 & \mathrm{c}\varphi & \mathrm{s}\varphi \\ 0 & e_1\mathrm{c}\varphi + 2\mathrm{s}\varphi & e_1\mathrm{s}\varphi - 2\mathrm{c}\varphi \end{bmatrix} \in \mathbb{R}^{3\times 3}, \tag{9}$$

where $\mathrm{c}\varphi \equiv \cos\varphi$ and $\mathrm{s}\varphi \equiv \sin\varphi$.

Next, taking the time derivative of $\boldsymbol{x}^*$ and using (8) one can obtain a relation between original, $\boldsymbol{u}$, and auxiliary, $\boldsymbol{v}$, input signals as follows

$$\boldsymbol{v} = \boldsymbol{T}(\boldsymbol{q}, \boldsymbol{e})\, \boldsymbol{u}, \tag{10}$$

where $\boldsymbol{T}(\boldsymbol{q}, \boldsymbol{e}) \in \mathbb{R}^{2\times 2}$ is the control transformation matrix defined as

$$\boldsymbol{T}(\boldsymbol{q}, \boldsymbol{e}) = \begin{bmatrix} 1 & 0 \\ L(\boldsymbol{q}, \boldsymbol{e}) & 1 \end{bmatrix}, \tag{11}$$

with $L(\boldsymbol{q}, \boldsymbol{e}) = -e_2 \sin\varphi + e_3 \cos\varphi$, such that $|L(\boldsymbol{q}, \boldsymbol{e})|$ means a projection of the distance between actual and desired position of the robot calculated in the direction perpendicular to the robot's heading.

Since $\boldsymbol{T}$ is globally invertible it is straightforward to get the following inverse formula which can be directly used for control design, namely

$$\boldsymbol{u} = \boldsymbol{T}^{-1}(\boldsymbol{q}, \boldsymbol{e})\, \boldsymbol{v}. \tag{12}$$

Summarizing, as a result of transformations (8) and (10) it is possible to solve the posture stabilization task for kinematics (1) by developing the control law which stabilizes the system given by (7). This approach is presented in the next subsection.

3.1.2 Control law development

The main concept of TVO stabilizer, as well as other controllers using transverse functions, consists of decreasing regulation error, $\boldsymbol{x}$, indirectly by tracking additional virtual signals $\boldsymbol{x}_d$.

Hence, taking into account system (7) the following signal $\boldsymbol{z} \in \mathbb{R}^3$ may be introduced

$$\boldsymbol{z} \triangleq \begin{bmatrix} \boldsymbol{z}^* \\ z_3 \end{bmatrix} = \boldsymbol{x} - \begin{bmatrix} \boldsymbol{x}_d \\ -\boldsymbol{x}_d^T \boldsymbol{J} \boldsymbol{x}^* \end{bmatrix}, \tag{13}$$

where $\boldsymbol{z}^* = [z_1\ z_2]^T \in \mathbb{R}^2$ and $\boldsymbol{x}_d = [x_{d1}\ x_{d2}]^T \in \mathbb{R}^2$ denote auxiliary time-varying bounded signals which will be defined later.

It is very important to note that relation (13) can be explained by means of differential geometry, since it determines a left-invariant group operation for the control system (7) (see works [17, 16]).

The auxiliary task of control consists of asymptotic (exponential) stabilization of (13) defined as

$$\forall_{\tau>0}\ \ \|\boldsymbol{z}\| \leqslant \gamma \|\boldsymbol{z}(0)\| \exp(-\beta\tau), \tag{14}$$

where γ and $\beta > 0$ are some positive constants.

According to (14) and definition (13) one can conclude that

$$\lim_{\tau\to\infty} \boldsymbol{z}^* = \boldsymbol{0} \Rightarrow \lim_{\tau\to\infty} \boldsymbol{x}^* = \boldsymbol{x}_d \tag{15}$$

and

$$\lim_{\tau\to\infty} z_3 = 0 \Rightarrow \lim_{\tau\to\infty} x_3 = 0. \tag{16}$$

These relations show that accuracy of regulation in the steady state is determined by signal $\boldsymbol{x}_d$. Moreover, $\boldsymbol{x}_d$ significantly influences transient behavior during regulation process since it is tracked by $\boldsymbol{x}^*$ according to (15). This problem will be discussed later.

In order to develop the control law asymptotically stabilizing $\boldsymbol{z}$ the following Lyapunov function candidate is proposed

$$V \triangleq \frac{1}{2}\boldsymbol{z}^T\boldsymbol{z}. \tag{17}$$

Next, taking the time derivative of V one can get

$$\dot{V} = \boldsymbol{z}^T\dot{\boldsymbol{z}} = \boldsymbol{z}^{*T}\dot{\boldsymbol{z}}^* + z_3\dot{z}_3. \tag{18}$$

Calculating the time derivative of $\boldsymbol{z}^*$ from (13) the following relation can be obtained

$$\dot{\boldsymbol{z}}^* = \boldsymbol{v} - \dot{\boldsymbol{x}}_d. \tag{19}$$

It should be noted that regulation task for the subsystem $\boldsymbol{z}^* = \boldsymbol{x}^* - \boldsymbol{x}_d$ is relatively easy and can be solved by using the following control signal

$$\boldsymbol{v} = -k_1\boldsymbol{z}^* + \dot{\boldsymbol{x}}_d, \tag{20}$$

where $k_1 > 0$ is a constant parameter. Using (20) and (13) in (18) yields

$$\dot{V} = -k_1\boldsymbol{z}^{*T}\boldsymbol{z}^* + z_3\dot{z}_3. \tag{21}$$

Next, the term $\dot{z}_3$ can be calculated according to (13) as follows (see details in Appendix)

$$\dot{z}_3 = \boldsymbol{x}_d^T\boldsymbol{J}\dot{\boldsymbol{x}}_d + 2k_1\boldsymbol{x}^{*T}\boldsymbol{J}\boldsymbol{x}_d. \tag{22}$$

Here signal $\dot{\boldsymbol{x}}_d$ can be interpreted as an additional control signal and can be used for asymptotic stabilization of coordinate z_3. In order to calculate $\dot{\boldsymbol{x}}_d$ we assume that $\boldsymbol{x}_d$ is originated by tunable oscillator [9] according to the following equation

$$\boldsymbol{x}_d = \boldsymbol{\Psi}\boldsymbol{\xi}, \tag{23}$$

where

$$\boldsymbol{\Psi} = \begin{bmatrix} \psi_1 & 0 \\ 0 & \psi_2 \end{bmatrix} \tag{24}$$

is a gain matrix with scalar functions $\psi_1(\tau)$ and $\psi_2(\tau) > 0$ which may be changed during regulation process and $\boldsymbol{\xi}$ is a solution of the following differential equation

$$\dot{\boldsymbol{\xi}} = u_\omega\boldsymbol{J}\boldsymbol{\xi} \tag{25}$$

with u_ω determining an instantaneous frequency of $\boldsymbol{\xi}$ and initial condition

$$\boldsymbol{\xi}(0)^T\boldsymbol{\xi}(0) = 1. \tag{26}$$

As one can see (25) describes an undamped linear oscillator with constant amplitude of signal $\boldsymbol{\xi}$, such that $\forall_{\tau>0}\ \boldsymbol{\xi}^T(\tau)\boldsymbol{\xi}(\tau) = 1$. Similarly to the control law given by Morin and Samson [17] frequency u_ω can be regarded as the third control signal (apart from v_1 and v_2) that makes the system to be virtually fully actuated.

An analytical formula describing u_ω can be obtained using the time derivative of (23), namely

$$\dot{\boldsymbol{x}}_d = \dot{\boldsymbol{\Psi}}\boldsymbol{\xi} + \boldsymbol{\Psi}\dot{\boldsymbol{\xi}} \tag{27}$$

and relations (22) and (20). A a result the following equation can be written

$$\dot{z}_3 = \boldsymbol{\xi}^T\boldsymbol{\Psi}^T\boldsymbol{J}\dot{\boldsymbol{\Psi}}\boldsymbol{\xi} + 2k_1\boldsymbol{x}^{*T}\boldsymbol{J}\boldsymbol{x}_d - \psi_1\psi_2u_\omega. \tag{28}$$

Now, it is straightforward to show that applying u_ω written as

$$u_\omega = \frac{-w + \boldsymbol{\xi}^T \boldsymbol{\Psi}^T \boldsymbol{J} \dot{\boldsymbol{\Psi}} \boldsymbol{\xi} + 2k_1 \boldsymbol{x}^{*T} \boldsymbol{J} \boldsymbol{x}_d}{\psi_1 \psi_2} \tag{29}$$

in (28) leads to decoupled subsystem, namely

$$\dot{z}_3 = w, \tag{30}$$

where w is a scalar function which is a new input. In order to ensure exponential stabilization of z_3 we propose to set

$$w = -k_2 z_3, \tag{31}$$

where $k_2 > 0$ is a constant controller parameter. Consequently, taking into account (31) and (30) allows to rewrite the time derivative of V as

$$\forall_{\tau>0, \|\boldsymbol{z}\| \neq 0} \; \dot{V} = -k_1 \boldsymbol{z}^{*T} \boldsymbol{z}^* - k_2 z_3^2 < 0. \tag{32}$$

Then, assuming that $\beta = \min\{k_1, k_2\}$ the following upper bound of $\dot{V}$ can be obtained

$$\dot{V} \leqslant -\beta \boldsymbol{z}^T \boldsymbol{z} = -2\beta V. \tag{33}$$

As a consequence one can prove that V tends to zero exponentially, namely

$$\forall_{\tau>0} \; V(\tau) = V(0) \exp(-2\beta\tau). \tag{34}$$

Proposition 1 *Assuming that k_1, k_2, ψ_1 and $\psi_2 > 0$, ψ_1, ψ_2, $\dot{\psi}_1$ and $\dot{\psi}_2 \in \mathcal{L}_\infty$, the controller given by (20), (29), (31), (23), (25) and (26) stabilizes system (13) exponentially in terms of (14).*

Proof 1 *The result given by Proposition 1 is a direct consequence of relation (34). However, to complete the proof it is necessary to show that all signals in the controlled system are bounded. Firstly, we examine frequency u_ω taking into account relation (29) and $\|\boldsymbol{\xi}\| = 1$. Then using the following relations*

$$\left| \boldsymbol{\xi}^T \boldsymbol{\Psi}^T \boldsymbol{J} \dot{\boldsymbol{\Psi}} \boldsymbol{\xi} \right| \leqslant \rho_1 \stackrel{\Delta}{=} \left| \dot{\psi}_1 \psi_2 - \psi_1 \dot{\psi}_2 \right| \in \mathcal{L}_\infty \tag{35}$$

and

$$\left| \boldsymbol{z}^{*T} \boldsymbol{J} \boldsymbol{x}_d \right| \leqslant \rho_2 \|\boldsymbol{z}^*\|, \tag{36}$$

with

$$\rho_2 \stackrel{\Delta}{=} \max\{\psi_1, \psi_2\} \in \mathcal{L}_\infty. \tag{37}$$

one can easily show that

$$|u_\omega| \leqslant \frac{k_2|z_3| + 2k_1\rho_2\|\boldsymbol{z}^*\| + \rho_1}{\psi_1\psi_2} \leqslant \rho_3 \frac{\|\boldsymbol{z}\| + \frac{\rho_1}{\rho_3}}{\psi_1\psi_2} \leqslant \rho_3 \frac{\|\boldsymbol{z}(0)\| \exp(-\beta\tau) + \frac{\rho_1}{\rho_3}}{\psi_1\psi_2}, \tag{38}$$

where $\rho_3 = \sqrt{2}\max\{k_1, 2k_2\rho_2\}$. As a consequence $u_\omega \in \mathcal{L}_\infty$ if only ψ_1 and ψ_2 satisfy the assumptions given by Proposition 1. Next considering $\dot{\boldsymbol{x}}_d$ it is easy to show (see (27)) that $u_\omega \in \mathcal{L}_\infty$ implies $\left\| \dot{\boldsymbol{\xi}} \right\| \in \mathcal{L}_\infty$ and consequently $\|\dot{\boldsymbol{x}}_d\| \in \mathcal{L}_\infty$. Finally, it is straightforward to conclude that $\|\boldsymbol{v}\| \in \mathcal{L}_\infty$. □

Considering (29) one can see that frequency of oscillation u_ω is strictly related to functions ψ_1 and ψ_2 which determine amplitude of auxiliary signal $\boldsymbol{x}_d$. Therefore, selection of these functions taking into account evolution of error $\boldsymbol{z}$ highly affects system behavior during transient states. In order to limit overshoots it is reasonable to choose $\psi_1\psi_2$ to be high enough that implies no-oscillatory behavior of the closed-loop system. On the other hand, according to (15) amplitude of $\boldsymbol{x}_d$ determines an accuracy of regulation in the steady-state. As a result high precision of regulation needs to assume $\lim_{\tau\to\infty} \psi_i(\tau) = \varepsilon_i$, where ε_i denotes a positive small constant (small enough for desired accuracy).

In order to do that, similarly to [9], the following gain functions $\psi_1(\tau)$ and $\psi_2(\tau)$ explicitly depending on time are proposed

$$\psi_i(\tau) = \psi_{i0} \exp(-\alpha_i \tau) + \varepsilon_i, \text{ for } i = 1, 2, \tag{39}$$

where $\psi_{i0} > 0$, $\alpha_i > 0$ and $\varepsilon_i > 0$ are scalar coefficients determining initial and limit value of the function ψ_i and its convergence rate, respectively. It is clear that, since functions (39) satisfy the assumptions of Proposition 1, the proof of it is still valid.

Considering tuning methods introduced by functions (39) one can prove according to (15) and (16) that

$$\lim_{\tau\to\infty} |x_1(\tau)| \leqslant \varepsilon_1, \quad \lim_{\tau\to\infty} |x_2(\tau)| \leqslant \varepsilon_2, \quad \lim_{\tau\to\infty} x_3(\tau) = 0. \tag{40}$$

Finally, we return to the stabilization problem of nonholonomic robot (1) in Cartesian space. According to error definition given by (4) and transformation (8) one can conclude that $\lim_{\tau\to\infty} \boldsymbol{x} = \boldsymbol{0}$ implies that $\lim_{\tau\to\infty} \boldsymbol{e} = \boldsymbol{0}$. Above considerations result in the following proposition:

Proposition 2 *Assuming that $\boldsymbol{\psi}_1$ and $\boldsymbol{\psi}_2$ are defined by (39) the controller given by (20), (29), (23), (25) and (26) with transformations (8) and (10) ensures boundness of the errors $\boldsymbol{e}$ in a sense that*

$$\lim_{\tau\to\infty} |e_1(\tau)| \leqslant \varepsilon_1, \quad \lim_{\tau\to\infty} \|\boldsymbol{e}^*(\tau)\| \leqslant \varepsilon_2 \sqrt{\frac{\varepsilon_1^2}{4} + 1}, \tag{41}$$

where $\boldsymbol{e}^* \triangleq [e_2 \; e_3]^T$.

Remark 1 *The convergence rate determined by α_i coefficient may be choosen arbitrary, at least from a theoretical point of view. However, taking into account (38) and considering the term written as*

$$\frac{\|\boldsymbol{z}(0)\| \exp(-\beta\tau)}{\psi_1\psi_2} \tag{42}$$

one can easily conclude that it decreases for all times if

$$\alpha_1 + \alpha_2 < \beta. \tag{43}$$

Hence, using this condition for selection of scaling functions ψ_1 and ψ_2 allows to prevent from increasing $|u_\omega|$ during regulation process.

Remark 2 *The exponential convergence of an auxiliary error $\boldsymbol{z}$ (see (14)) implies exponential convergence of the transformed state vector $\boldsymbol{x}$ to a neighborhood of desired point with radius determined by $\boldsymbol{\varepsilon}_i$ (compare also [9]). Consequently, considering inverse transformation $\boldsymbol{P}^{-1}$ one can deduce a similar conclusion governing convergence of error $\boldsymbol{e}$. Moreover, the convergence rate can be determined easily, since it is directly related to the selection of k_1, k_2 as well as α_i parameters (compare (34) and (39)).*

Remark 3 *Assuming that* $\varepsilon_i \equiv 0$ *and* $\dot{\psi}_1\psi_2 = \psi_1\dot{\psi}_2$ *which yields to* $\rho_1 = 0$*, then it is possible to obtain asymptotic convergence result in Cartesian space. It can be easily proved using (38) that* $|u_\omega|$ *remains bounded for all times if only condition (43) is satisfied. However, this result is based on the fact that for initial condition* $\|\boldsymbol{z}(0)\| > 0$ *the closed-loop system will never reach equilibrium point in finite time. Hence, the controller considered here does not asymptotically stabilize the system at the origin. It means that if* $\|\boldsymbol{z}(0)\| > 0$ *it is necessary to select* $\psi_1\psi_2 > 0$ *in order to avoid singularity. Therefore, in the case when* $\varepsilon_i \equiv 0$ *the control law considered here is time-differentiable everywhere except the origin.*

3.1.3 Simplified version of the controller

As one can see for the TVO controller terms concerning time-derivatives of ψ_1 and ψ_2 are used explicitly. However, it would be simpler to neglect these terms which allows to change ψ_i during regulation without calculating their time-derivatives. Moreover, it was observed during extensive simulations that neglecting $\dot{\psi}_i$ in the control law may result in less oscillatory behavior. This phenomena can be explained taking into account numerator of expression (29). Since the following inequality holds

$$\left|-w + 2k_1\boldsymbol{x}^{*T}\boldsymbol{J}\boldsymbol{x}_d\right| + \left|\boldsymbol{\xi}^T\boldsymbol{\Psi}^T\boldsymbol{J}\dot{\boldsymbol{\Psi}}\boldsymbol{\xi}\right| \geqslant \left|-w + 2k_1\boldsymbol{x}^{*T}\boldsymbol{J}\boldsymbol{x}_d\right| \tag{44}$$

removing the term $\boldsymbol{\xi}^T\boldsymbol{\Psi}^T\boldsymbol{J}\dot{\boldsymbol{\Psi}}\boldsymbol{\xi}$ should result in lower upper bound of $|u_\omega|$.

This statement is illustrated in Fig. 2 for exponential scaling of ψ_i. The controller parameters were selected as: $k_1 = k_2 = 10$, $\boldsymbol{\xi}(0) = \frac{\sqrt{2}}{2}[1\ 1]^T$, $\psi_1(0) = \psi_2(0) = 0.5$, $\alpha_1 = \alpha_2 = 5$ and $\varepsilon_1 = \varepsilon_2 = 0.05$. As one can see convergence rate in both cases is quite

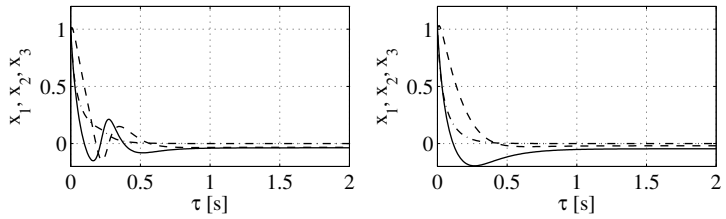

Figure 2: Stabilization errors for TVO controller obtained for nonholonomic integrator: x_1(–), x_2(- -) and x_3(-.-). Left: original controller, right: simplified controller (without using $\dot{\boldsymbol{\Psi}}$ in control law).

similar, but if matrix $\dot{\boldsymbol{\Psi}}$ is used explicitly the transient behavior appears to be more oscillatory than in case when $\dot{\boldsymbol{\Psi}}$ is dropped. Note, that the steady-state errors in both cases are limited to the nonzero values and are in the same assumed neighborhood of the origin if only $\lim_{\tau\to\infty}\dot{\boldsymbol{\Psi}}(\tau) = \boldsymbol{0} \in \mathbb{R}^{2\times 2}$.

As a consequence based on presented observation the following proposition can be justified:

Proposition 3 *Assuming that gain coefficients* $k_1, k_2 > 0.5$*,* $\psi_i > 0$ *and* $\dot{\psi}_i$ *can be lower bounded by time-varying exponentially function such that* $\lim_{\tau\to\infty}\dot{\psi}_i(\tau) = 0$ *the modified control law written as*

$$\boldsymbol{v} = -k_1\boldsymbol{z}^* + \boldsymbol{\Psi}\dot{\boldsymbol{\xi}}, \tag{45}$$

$$u_\omega = \frac{k_2 z_3 + 2k_1\boldsymbol{z}^{*T}\boldsymbol{J}\boldsymbol{x}_d}{\psi_1\psi_2} \tag{46}$$

ensures exponential convergence of $\boldsymbol{z}$.

Proof 2 *In order to show stability of system (13) we use the positive scalar function defined by (17). Then calculating its time derivative and using (45)-(46) one can get*

$$\dot{V} = -k_1 \boldsymbol{z}^{*T} \boldsymbol{z}^* - k_2 z_3^2 - \boldsymbol{z}^{*T} \dot{\boldsymbol{\Psi}} \boldsymbol{\xi} + z_3 \boldsymbol{\xi}^T \boldsymbol{\Psi}^T \boldsymbol{J} \dot{\boldsymbol{\Psi}} \boldsymbol{\xi}. \tag{47}$$

One can easily conclude that signs of terms $\boldsymbol{z}^{*T} \dot{\boldsymbol{\Psi}} \boldsymbol{\xi}$ *and* $\boldsymbol{\xi}^T \boldsymbol{\Psi}^T \boldsymbol{J} \dot{\boldsymbol{\Psi}} \boldsymbol{\xi}$ *are not determined. Hence, we may find upper bound of them using relation (36) and*

$$\boldsymbol{z}^{*T} \dot{\boldsymbol{\Psi}} \boldsymbol{\xi} \leqslant \rho_4 \left\| \boldsymbol{z}^* \right\|, \tag{48}$$

where

$$\rho_4 \triangleq \max \left\{ \left| \dot{\psi}_1 \right|, \left| \dot{\psi}_2 \right| \right\}. \tag{49}$$

Consequently $\dot{V}$ *satisfies*

$$\dot{V} \leqslant -k_1 \left\| \boldsymbol{z}^* \right\|^2 - k_2 z_3^2 + \rho_4 \left\| \boldsymbol{z}^* \right\| + \rho_1 \left| z_3 \right| \tag{50}$$

with ρ_1 *defined by (35).*

Introducing upper bound of last two terms as

$$\rho_4 \left\| \boldsymbol{z}^* \right\| \leqslant \tfrac{1}{2} \rho_4^2 + \tfrac{1}{2} \left\| \boldsymbol{z}^* \right\|^2, \quad \rho_1 \left| z_3 \right\| \leqslant \tfrac{1}{2} \rho_1^2 + \tfrac{1}{2} z_3^2 \tag{51}$$

implies that

$$\dot{V} \leqslant \left(-k_1 + 0.5 \right) \left\| \boldsymbol{z}^* \right\|^2 + \left(-k_2 + 0.5 \right) z_3^2 + 0.5 \left(\rho_4^2 + \rho_1^2 \right). \tag{52}$$

Next, redefining β *as*

$$\beta \triangleq \min \left\{ k_1 - 0.5, \ k_2 - 0.5 \right\} \tag{53}$$

and defining

$$\rho_5^2(\tau) \triangleq 0.5 \left(\rho_4^2 + \rho_1^2 \right) \leqslant \rho_5^2 \left(0 \right) \exp \left(-2 \alpha_{max} \tau \right), \tag{54}$$

where $\alpha_{max} \triangleq \max\{\alpha_1, \alpha_2\}$ *yields*

$$\dot{V} \leqslant \beta \left\| \boldsymbol{z} \right\|^2 + 0.5 \rho_5^2 \left(0 \right) \exp \left(-2 \alpha_{max} \tau \right). \tag{55}$$

Then time-derivative of V *becomes*

$$\dot{V} \leqslant 2 \beta V + \rho_5^2 \left(0 \right) \exp \left(-2 \alpha_{max} \tau \right). \tag{56}$$

Next calculating a solution of inequality (56) (see Appendix) one can obtain that

$$V \left(\tau \right) \leqslant V \left(0 \right) \exp \left(-2 \beta \tau \right) + \frac{0.5 \rho_5^2}{\beta - \alpha_{max}} \left[\exp \left(-2 \alpha_{max} \tau \right) - \exp \left(-2 \beta \tau \right) \right], \tag{57}$$

where an assumption that $\beta \neq \alpha_{max}$ *has been used. This result leads to the following upper bound of* $\left\| \boldsymbol{z} \left(\tau \right) \right\|$*, namely*

$$\left\| \boldsymbol{z} \left(\tau \right) \right\| \leqslant \left\| \boldsymbol{z} \left(0 \right) \right\| \exp \left(-\beta \tau \right) + \frac{\sqrt{2}}{2} \rho_5 \sqrt{\frac{\exp \left(-2 \alpha_{max} \tau \right) - \exp \left(-2 \beta \tau \right)}{\beta - \alpha_{max}}}. \tag{58}$$

From (58) one can conclude that tracking error $\left\| \boldsymbol{z} \left(\tau \right) \right\|$ *tends to zero as time goes to infinity (at the limit disturbance term under square root disappears) in spite of fact that scalar function* V *is not globally decreasing for all initial conditions* $\left\| \boldsymbol{z} \left(0 \right) \right\|$ *(note that* $\dot{V}$ *may be positive in some time interval).*

Next, based on stability result given by (58) and making calculations similar to ones presented in proof of Proposition 1 it is clear to see that $\left\| \boldsymbol{v} \right\|, u_\omega \in \mathcal{L}_\infty$ *if* $\psi_i, \dot{\psi}_i \in \mathcal{L}_\infty$.
□

Remark 4 *Assuming that k_1 and k_2 are selected properly in order to satisfy (43), while β is defined by (53) the upper bound of $|u_\omega|$ decreases during regulation process. Hence, the maximal value $|u_\omega|$ can be estimated by calculating $|u_\omega(0)|$ as follows (for simplicity it is supposed that $\rho_3 = 2\sqrt{2}k_1\rho_2$ and $\varepsilon_1 = \varepsilon_2 \approx 0$ are negligible with respect to ψ_{10} and ψ_{20})*

$$|u_{\omega max}| \leqslant 2\sqrt{2}k_1 \|\boldsymbol{z}(0)\| \frac{\psi_{max0}}{\psi_{min0}^2}, \tag{59}$$

where $\psi_{min0} \triangleq \min\{\psi_{10}, \psi_{20}\}$, $\psi_{max0} \triangleq \max\{\psi_{10}, \psi_{20}\}$.

According to this result one can chose ψ_{10} and ψ_{20} high enough in order to limit oscillatory behavior during transient states. On the other hand selection of high values ψ_{10} or ψ_{20} may lead to high error at the beginning of regulation process according to assumption (13). Moreover, for typical applications, since ψ_1 shapes orientation error (compare (13) and (8)), it is reasonable to choose $\psi_{10} \leqslant \pi$.

It should also be mentioned that transient states are dependent on selection of $\boldsymbol{\xi}(0)$ which determines an initial direction of convergence of vector $\boldsymbol{x}^*$ in auxiliary state space. As a result different $\boldsymbol{\xi}(0)$ leads to different paths of the robot observed in Cartesian space, namely it can move forward or backward, with one turn or more, etc.

3.1.4 Control scaling

In many control applications saturation of input signals exists. Therefore, developing the controller without taking into account this limitation may not guarantee good results (see for example [20, 21]).

Here, we consider a method to rescale control signal for TVO controller used for stabilization of affine driftless system. The presented algorithm can be used to decrease or increase value of control signals (in this case both amplitudes and frequency) without lack of stability from a theoretical point of view. It may be useful to scale control signal to be within range of permissible values.

Firstly, let us assume that original control signal $\boldsymbol{v}$ calculated according to (45) is rescaled by some positive scalar function $\mu(\tau) \in \mathcal{L}_\infty$ as

$$\boldsymbol{v}(\tau) = \mu(\tau)\left[-k_1\boldsymbol{z}^*(\tau) + \boldsymbol{\Psi}(\tau_s)\boldsymbol{J}\boldsymbol{\xi}(\tau_s)u_\omega(\tau)\right] \tag{60}$$

with

$$u_\omega(\tau) = \frac{k_2 z_3(\tau) + 2k_1\boldsymbol{z}^{*T}(\tau)\boldsymbol{J}\boldsymbol{\Psi}(\tau_s)\boldsymbol{\xi}(\tau_s)}{\psi_1(\tau_s)\psi_2(\tau_s)} \tag{61}$$

where

$$\tau_s \triangleq \tau_s(\tau) \triangleq \int_0^\tau \mu(\sigma)\, d\sigma \tag{62}$$

denotes scaled time. It should be noted that introducing time scaling affects only auxiliary variables depending explicitly on time, namely related with signal $\boldsymbol{x}_d$. Therefore, at instant time τ, $\boldsymbol{x}_d$ and consequently $\boldsymbol{\xi}$ and $\boldsymbol{\Psi}$ are calculated at τ_s. Accordingly, in definition of $\boldsymbol{z}(\tau)$ (see equation (13)) $\boldsymbol{x}_d(\tau)$ is replaced by $\boldsymbol{x}_d(\tau_s)$. This proposition is a result of using frequency of $\boldsymbol{\xi}$ as a third control signal. Hence, rescaling physical input $\boldsymbol{v}$ must result in proportional scaling $\dot{\boldsymbol{\xi}}$, that simply leads to introduction the virtual time τ_s.

As one can prove introducing time-scaling with respect to $\boldsymbol{x}_d$ yields

$$\dot{\boldsymbol{\xi}}(\tau_s(\tau)) = \mu(\tau)\frac{d}{d\tau_s}\boldsymbol{\xi}(\tau_s), \quad \dot{\boldsymbol{\Psi}}(\tau_s(\tau)) = \mu(\tau)\frac{d}{d\tau_s}\boldsymbol{\Psi}(\tau_s), \tag{63}$$

where $\boldsymbol{\xi}(\tau_s)$ denotes a solution of oscillator equation determined for time τ_s, namely

$$\frac{d}{d\tau_s}\boldsymbol{\xi} = u_\omega(\tau)\,\boldsymbol{J}\boldsymbol{\xi}(\tau_s). \tag{64}$$

Substituting equations (60)-(61) to (19) and (22) allows to show that time-derivative of $\boldsymbol{z} = \left[\boldsymbol{z}^{*T}\ z_3\right]^T$ becomes

$$\dot{\boldsymbol{z}}^*(\tau) = \mu\left[-k_1\boldsymbol{z}^*(\tau) - \frac{d}{d\tau_s}\boldsymbol{\Psi}(\tau_s)\,\boldsymbol{\xi}(\tau_s)\right] \tag{65}$$

and

$$\dot{z}_3 = \mu\left[-k_2 z_3(\tau) + \boldsymbol{\xi}^T(\tau_s)\,\boldsymbol{\Psi}^T(\tau_s)\,\frac{d}{d\tau_s}\boldsymbol{\Psi}(\tau_s)\,\boldsymbol{\xi}(\tau_s)\right]. \tag{66}$$

Next, it is straightforward to prove that

$$\begin{aligned}\dot{V} = \mu\Big[&-k_1\left\|\boldsymbol{z}^*(\tau)\right\|^2 - k_2 z_3^2(\tau) - \boldsymbol{z}^{*T}(\tau)\,\frac{d}{d\tau_s}\boldsymbol{\Psi}(\tau_s)\,\boldsymbol{\xi}(\tau_s) + \\ &+ z_3(\tau_s)\,\boldsymbol{\xi}^T(\tau_s)\,\boldsymbol{\Psi}^T(\tau_s)\,\boldsymbol{J}\frac{d}{d\tau_s}\boldsymbol{\Psi}(\tau_s)\,\boldsymbol{\xi}(\tau_s)\Big].\end{aligned} \tag{67}$$

Similarly to calculation made in the proof of Proposition 3 one can prove that

$$\forall_{\tau>0}\ V(\tau) \leqslant V(0)\exp(-2\mu\beta\tau) + \frac{0.5\rho_5^2(\tau_s)}{\beta-\alpha_{max}}\left[\exp(-2\alpha_{max}\tau_s) - \exp(-2\beta\tau_s)\right]. \tag{68}$$

Finally, one can conclude that convergence of function V can be changed proportionally to μ. Moreover, in the same way the time evolution of $\boldsymbol{\xi}$ and $\boldsymbol{\Psi}$ is rescaled (compare (63). Hence, $\boldsymbol{z}$ may evolve faster (for $\mu > 1$) or slower (for $0 < \mu < 1$) with respect to the original solution (i.e. when $\mu = 1$). It is very important to note that shape of trajectory describing evolution of $\boldsymbol{z}$ in the state space is independent on choosing $\mu > 0$.

Remark 5 *Signal and time scaling presented here seems to be very effective solution for controlling driftless system. Using properly scaling function μ one can easily make regulation to be faster or slower in order to avoid control signal saturation and limit its frequency. Consequently, it is simpler to tune the controller in order to obtain non-oscillatory results theoretically and next rescale the control signal taking into account control limitations which affect physical object.*

3.2 Control law based on Vector Field Orientation approach

Now, the problem of asymptotic stabilization (in the sense of definition 1) will be considered. Without lack of generality we assume, that the reference point is at the origin:

$$\boldsymbol{q}_t \stackrel{\Delta}{=} [0\ 0\ 0]^T. \tag{69}$$

In the next section the Vector Field Orientation (VFO) approach will be described. It allows to derive a simple controller, which makes the posture error (4) asymptotically converge to zero. The VFO strategy for the unicycle robot has been introduced for the first time in [12].

3.2.1 VFO approach

The VFO concept directly comes from an intuitive geometrical interpretation of the structure of controlled kinematics (1) and its possible time evolution in a response to specific controls $u_1(\cdot)$ and $u_2(\cdot)$. The main idea involves decomposition of Eq. (1) into two subsystems Σ_1 and Σ_2:

$$\Sigma_1: \quad \dot{\varphi} = u_1, \tag{70}$$

$$\Sigma_2: \quad \dot{\boldsymbol{q}}^* = \boldsymbol{g}_2^*(\boldsymbol{q})u_2, \quad \text{where} \quad \dot{\boldsymbol{q}}^* \triangleq \begin{bmatrix} \dot{x} \\ \dot{y} \end{bmatrix}, \ \boldsymbol{g}_2^*(\boldsymbol{q}) \triangleq \begin{bmatrix} \cos\varphi \\ \sin\varphi \end{bmatrix}. \tag{71}$$

The first 1-D subsystem is linear. The second one (2-D) is highly nonlinear. One can find, that the direction of time evolution of state variables x, y in $\mathbb{R}^2$ depends on the direction of the vector field $\boldsymbol{g}_2^*(\boldsymbol{q})$:

$$Dir\{\dot{\boldsymbol{q}}^*\} = Dir\{\boldsymbol{g}_2^*(\boldsymbol{q})\}, \tag{72}$$

where $\dot{\boldsymbol{q}}^* \triangleq [\dot{x}\ \dot{y}]^T$ and $Dir\{\boldsymbol{\zeta}\}$ denotes the direction of $\boldsymbol{\zeta}$ in $\mathbb{R}^N$ (here in $\mathbb{R}^2$). Since both components of $\boldsymbol{g}_2^*(\boldsymbol{q})$ depend on the first state variable φ, the current direction (and orientation[1]) of $\boldsymbol{g}_2^*(\boldsymbol{q})$ can be changed by changing the actual value of φ. From (70) it results, that this change can be accomplished relatively easily with the first input signal u_1. Due to the particular form of the vector field $\boldsymbol{g}_2^*(\boldsymbol{q})$ in (71), all accessible directions in $\mathbb{R}^2$ as a function of φ variable include all possible directions on the plane. Therefore, one can say, that $\boldsymbol{g}_2^*(\boldsymbol{q})$ is fully orientable in $\mathbb{R}^2$. Since φ directly affects the orientation of $\boldsymbol{g}_2^*(\boldsymbol{q})$, it can be called the *orienting variable*. Since input u_1 directly drives the orienting variable φ, it can be called the *orienting control*. It is easy to find, that the second input u_2 drives the sub-state $\boldsymbol{q}^* \triangleq [x\ y]^T$ along the current direction of $\boldsymbol{g}_2^*(\boldsymbol{q})$. One can say, that u_2 *pushes* the sub-state $\boldsymbol{q}^*$ along this vector field. Hence u_2 will be called the *pushing control*. Proposed interpretation and terminology allows to describe the VFO control methodology for the system described by (70) and (71). First we have to introduce an additional vector field

$$\boldsymbol{h}(\boldsymbol{e}(\tau)) \triangleq \begin{bmatrix} h_1(\boldsymbol{e}(\tau)) \\ h_2(\boldsymbol{e}(\tau)) \\ h_3(\boldsymbol{e}(\tau)) \end{bmatrix} \triangleq \begin{bmatrix} h_1(\boldsymbol{e}(\tau)) \\ \boldsymbol{h}^*(\boldsymbol{e}(\tau)) \end{bmatrix} \in \mathbb{R}^3, \tag{73}$$

which will be called the *convergence vector field*. Let us assume, that this vector determines an instantaneous convergence direction (orientation), which should be followed by a controlled system to reach the reference goal point $\boldsymbol{q}_t$. At the moment we assume, that $\boldsymbol{h}$ is given. The VFO control strategy can be explained as follows.

Since $\boldsymbol{h}$ defines the convergence direction (and orientation), it is desirable to put the direction (orientation) of the generalized velocity vector field $\dot{\boldsymbol{q}}$ of the controlled system (1) onto direction of $\boldsymbol{h}$. As it will be shown, one can accomplish this task by the first input u_1. Simultaneously, the subsystem (71) should be pushed by the second input u_2, along the being oriented vector field $\dot{\boldsymbol{q}}^*$. Moreover, it seems to be reasonable to push the subsystem (71) only proportionally to a current orthogonal projection of $\boldsymbol{h}^* \triangleq [h_2\ h_3]^T$ onto the instantaneous direction of $\boldsymbol{g}_2^*(\boldsymbol{q})$ (or of $\dot{\boldsymbol{q}}^*$ due to (72)). As far as a convergence of variable φ is concerned, the whole vector field $\boldsymbol{h}$ should be designed, to guarantee

[1] Strictly speaking, the *orientation* of some vector field $\boldsymbol{\zeta}$ means its *direction* in $\mathbb{R}^N$ along with its sense.

tending of φ to its reference value at the limit as x and y reach their reference values. Mathematically, the VFO strategy explained above can be written in the following form:

$$\begin{aligned} &\textit{find } u_1 \;\; : \;\; \left\{ \lim_{\tau\to\infty} \dot{\boldsymbol{q}}(\tau) \,||\, \boldsymbol{h}(\boldsymbol{e}(\tau)) \;\Leftrightarrow\; \lim_{\tau\to\infty} \dot{\boldsymbol{q}}(\tau)\, k(\tau) = \boldsymbol{h}(\boldsymbol{e}(\tau)) \right\}, \\ &\textit{find } u_2 \;\; : \;\; \{ \,\| \dot{\boldsymbol{q}}^* \| \propto \| \boldsymbol{h}^* \| \cos\alpha \}, \end{aligned}$$

where $k(\tau) \neq 0$ is a scalar function, $\alpha \triangleq \angle(\boldsymbol{g}_2^*(\boldsymbol{q}), \boldsymbol{h}^*)$, the expression $\boldsymbol{a} \,||\, \boldsymbol{b}$ denotes, that both vector fields $\boldsymbol{a}$ and $\boldsymbol{b}$ are parallel, and $\propto$ is a proportionality operator. According to the VFO strategy, conditions, which ensure matching of directions of two vector fields $\boldsymbol{h}$ and $\dot{\boldsymbol{q}}$, will be derived. For, the first of above relations can be rewritten as follows (for simplicity some arguments are omitted):

$$\textit{find } u_1 \;\; : \;\; \left\{ \lim_{\tau\to\infty} \begin{bmatrix} \dot{\varphi}(\tau) \\ \dot{x}(\tau) \\ \dot{y}(\tau) \end{bmatrix} k(\tau) = \begin{bmatrix} h_1 \\ h_2 \\ h_3 \end{bmatrix} \;\overset{(1)}{\Rightarrow}\; \lim_{\tau\to\infty} \begin{bmatrix} u_1 k(\tau) \\ \cos\varphi(\tau) u_2 k(\tau) \\ \sin\varphi(\tau) u_2 k(\tau) \end{bmatrix} = \begin{bmatrix} h_1 \\ h_2 \\ h_3 \end{bmatrix} \right\}$$

Combining the last two relations, one obtains two so-called *VFO orienting conditions*:

$$\textit{find } u_1 \;\; : \;\; \left\{ \begin{array}{c} u_1\, k(\tau) = h_1 \\ \lim\limits_{\tau\to\infty} \varphi(\tau) = \mathrm{Atan2}\left(sgn(k(\tau))h_3, sgn(k(\tau))h_2\right) \end{array} \right\}, \tag{74}$$

where $\mathrm{Atan2}\,(.,.)$ denotes the four-quadrant inverse tangent function and:

$$sgn(a) \triangleq \left\{ \begin{array}{rll} 1\,, & \text{for} & a \geqslant 0, \\ -1\,, & \text{for} & a < 0. \end{array} \right. \tag{75}$$

Conditions (74) should be met to ensure placing direction of $\dot{\boldsymbol{q}}$ onto direction of $\boldsymbol{h}$ and will be directly used in the sequel for design purposes of the first control signal u_1. Function $k(\tau)$, which appears in the above conditions is not needed to be known explicitly[2], however its sign will be helpful to properly shape transient states of the whole control system. We postulate the following equality:

$$sgn(k(\tau)) \triangleq sgn(e_{20}), \tag{76}$$

where $e_{20} \equiv e_2(0)$ denotes the initial value of the error $e_2(\tau) \overset{(4)}{=} x_t - x(\tau)$.

3.2.2 VFO controller

By appropriate definition of signal u_1, the first relation in (74) can be fulfilled instantaneously. The second one, however, can be generally met only at the limit as $\tau \to \infty$. Hence we introduce an *auxiliary orientation variable*:

$$\varphi_d \triangleq \mathrm{Atan2}\left(sgn(e_{20})h_3, sgn(e_{20})h_2\right) \tag{77}$$

and the *auxiliary orientation error*:

$$e_{1d} \triangleq \varphi_d - \varphi. \tag{78}$$

Now, to meet the second condition in (74) it suffices, to show that the error e_{1d} tends to zero. Therefore, we propose to define the first component of the convergence vector as follows:

$$h_1(\boldsymbol{e}(\tau)) \triangleq k(\tau)[k_1 e_{1d} + \dot{\varphi}_d], \tag{79}$$

[2] As it will be shown, function $k(\tau)$ does not appear in the final definition of control signals.

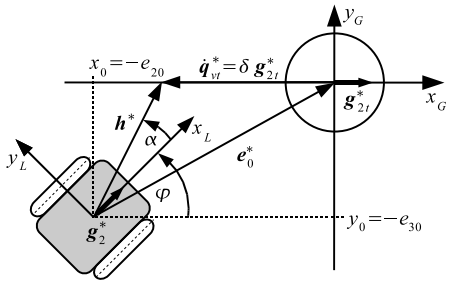

Figure 3: Mobile robot during the VFO control process for $k_p = 1$, $\boldsymbol{q}_t = [0\ 0\ 0]^T$ and $\delta = -\eta \,\|\, \boldsymbol{e}^* \|\, sgn(e_{20})$.

where $k_1 > 0$ is a design coefficient and feedforward term can be computed as follows

$$\dot{\varphi}_d \overset{(77)}{=} \frac{\dot{h}_3 h_2 - h_3 \dot{h}_2}{h_2^2 + h_3^2}, \qquad h_2^2 + h_3^2 \neq 0, \tag{80}$$

where the terms $\dot{h}_2$ and $\dot{h}_3$ are determined in Appendix. Finally, to meet the first relation in (74), it suffices to take:

$$u_1 \triangleq \frac{h_1}{k(\tau)} \overset{(79)}{=} k_1 e_{1d} + \dot{\varphi}_d. \tag{81}$$

Derived control law (81) should guarantee that: $\lim_{\tau\to\infty} e_{1d} = 0$ (it will be proved in the sequel).

Now the two last components h_2 and h_3 of a the convergence vector field $\boldsymbol{h}$ will be defined. Let us introduce the following proposition:

$$\boldsymbol{h}^*(\boldsymbol{e}(\tau)) = \begin{bmatrix} h_2(\boldsymbol{e}(\tau)) \\ h_3(\boldsymbol{e}(\tau)) \end{bmatrix} \triangleq k_p \boldsymbol{e}^* + \dot{\boldsymbol{q}}^*_{vt}, \quad \boldsymbol{e}^* \triangleq \begin{bmatrix} e_2 \\ e_3 \end{bmatrix}, \tag{82}$$

where $k_p > 0$ is a design coefficient. The last term $\dot{\boldsymbol{q}}^*_{vt}$ is called as the *virtual reference velocity* and is defined as follows

$$\dot{\boldsymbol{q}}^*_{vt} \triangleq -\eta \,\|\, \boldsymbol{e}^* \|\, sgn(e_{20})\, \boldsymbol{g}^*_{2t}, \qquad 0 < \eta < k_p, \tag{83}$$

where

$$\boldsymbol{g}^*_{2t} \triangleq \boldsymbol{g}^*_2(\boldsymbol{q}_t) \overset{(71)}{=} \begin{bmatrix} \cos\varphi_t \\ \sin\varphi_t \end{bmatrix} \overset{(69)}{=} \begin{bmatrix} 1 \\ 0 \end{bmatrix}. \tag{84}$$

It will be shown, that the additional coefficient η in (83) will be helpful in shaping transient states (see Fig. 3).

According to VFO strategy it remains to define the pushing control u_2. Recalling consideration conducted in Section 3.2.1 we propose to take:

$$u_2 \triangleq \|\, \boldsymbol{h}^* \| \cos\alpha, \tag{85}$$

where $\alpha \triangleq \angle(\boldsymbol{g}^*_2, \boldsymbol{h}^*)$ and hence

$$\cos\alpha \triangleq \frac{\boldsymbol{g}^{*T}_2\, \boldsymbol{h}^*}{\|\, \boldsymbol{g}^*_2 \|\, \|\, \boldsymbol{h}^* \|} \qquad \text{for} \quad \|\, \boldsymbol{h}^* \| \neq 0. \tag{86}$$

Substituting (86) into (85) allows to obtain simpler form of control signal u_2:

$$u_2 = \frac{\boldsymbol{g}^{*T}_2\, \boldsymbol{h}^*}{\|\, \boldsymbol{g}^*_2 \|} \overset{(1)}{=} h_2 \cos\varphi + h_3 \sin\varphi. \tag{87}$$

Now, we can formulate the following proposition.

Proposition 4 *Given the reference point (69). Assuming that:* $\boldsymbol{e}^*(0) \in \mathbb{R}^2 \setminus \mathbf{0}$ *and* $\forall_{\tau<\infty} \| \boldsymbol{h}^*(\boldsymbol{e}(\tau))\| \neq 0$*, the VFO controller (81) and (87) guarantees asymptotic convergence of the posture error (4) to zero as* $\tau \to \infty$*.*

Proof. First, let us consider the *orienting variable* φ behavior. Substituting (81) to (1) yields:

$$\dot{e}_{1d} + k_1 e_{1d} = 0. \tag{88}$$

One concludes, that the orienting variable φ exponentially tends to the auxiliary direction angle φ_d:

$$\lim_{\tau\to\infty} e_{1d}(\tau) = 0. \tag{89}$$

Now we will take into account the position error $\boldsymbol{e}^*$. For the posture stabilization task we have:

$$\boldsymbol{e}^* \stackrel{\Delta}{=} \boldsymbol{q}_t^* - \boldsymbol{q}^* \quad \Rightarrow \quad \dot{\boldsymbol{e}}^* = -\dot{\boldsymbol{q}}^*. \tag{90}$$

Using (82) one can rewrite the above right hand side equation as follows: $\dot{\boldsymbol{e}}^* = -\dot{\boldsymbol{q}}^* + \boldsymbol{h}^* - k_p \boldsymbol{e}^* - \dot{\boldsymbol{q}}_{vt}^*$, which can be ordered in the following way:

$$\dot{\boldsymbol{e}}^* + k_p \boldsymbol{e}^* = \boldsymbol{r} - \dot{\boldsymbol{q}}_{vt}^*, \qquad \boldsymbol{r} \stackrel{\Delta}{=} \boldsymbol{h}^* - \dot{\boldsymbol{q}}^*. \tag{91}$$

Making simple calculations (see Appendix) one may derive the following useful relation:

$$\| \boldsymbol{r}\|^2 = \| \boldsymbol{h}^*\|^2 (1 - \cos^2 \alpha), \tag{92}$$

where $\cos\alpha$ is defined by (86) and (see Appendix)

$$\lim_{\varphi\to\varphi_d} (1 - \cos^2 \alpha) = 0. \tag{93}$$

Now, we introduce the following positive-definite Lyapunov function candidate: $V(\boldsymbol{e}^*) \stackrel{\Delta}{=} \frac{1}{2}\boldsymbol{e}^{*T}\boldsymbol{e}^*$. Time derivative of this function can be estimated as follows (to simplify the notation, we use $\gamma = \sqrt{1 - \cos^2\alpha} \ \in [0, 1]$ and $\delta = -\eta \| \boldsymbol{e}^*\| \, sgn(e_{20})$):

$$\begin{aligned}
\dot{V} &= \boldsymbol{e}^{*T}\dot{\boldsymbol{e}}^* \stackrel{(91)}{=} \boldsymbol{e}^{*T} (-k_p \boldsymbol{e}^* + \boldsymbol{r} - \dot{\boldsymbol{q}}_{vt}^*) \stackrel{(83)}{=} \boldsymbol{e}^{*T} (-k_p \boldsymbol{e}^* + \boldsymbol{r} - \delta \, \boldsymbol{g}_{2t}^*) = \\
&= -k_p \| \boldsymbol{e}^*\|^2 + \boldsymbol{e}^{*T}\boldsymbol{r} - \delta \boldsymbol{e}^{*T}\boldsymbol{g}_{2t}^* \leqslant -k_p \| \boldsymbol{e}^*\|^2 + \| \boldsymbol{e}^*\| \, \| \boldsymbol{r}\| + |\delta| \, \| \boldsymbol{e}^*\| \, \| \boldsymbol{g}_{2t}^*\| = \\
&\stackrel{(84)}{=} -k_p \| \boldsymbol{e}^*\|^2 + \| \boldsymbol{e}^*\| \, \| \boldsymbol{r}\| + |\delta| \, \| \boldsymbol{e}^*\| = \\
&\stackrel{(92)}{=} -k_p \| \boldsymbol{e}^*\|^2 + \| \boldsymbol{e}^*\| \, \| \boldsymbol{h}^*\| \, \gamma + |\delta| \, \| \boldsymbol{e}^*\| = \\
&\stackrel{(82)}{=} -k_p \| \boldsymbol{e}^*\|^2 + \| \boldsymbol{e}^*\| \, [\, \| k_p \boldsymbol{e}^* + \dot{\boldsymbol{q}}_{vt}^*\| \, \gamma + |\delta| \,] \leqslant \\
&\leqslant -k_p \| \boldsymbol{e}^*\|^2 + \| \boldsymbol{e}^*\| \, [\, (k_p \| \boldsymbol{e}^*\| + |\delta|)\gamma + |\delta| \,] = \\
&= -k_p (1 - \gamma) \| \boldsymbol{e}^*\|^2 + |\delta| \, (1 + \gamma) \| \boldsymbol{e}^*\| = -[k_p - k_p\gamma - \eta - \eta\gamma] \| \boldsymbol{e}^*\|^2 \ .
\end{aligned}$$

The above time derivative is negative-definite, if the term in brackets is positive. It gives the following convergence condition:

$$\gamma < (k_p - \eta)/(k_p + \eta) \quad \Rightarrow \quad \lim_{\tau\to\infty} \| \boldsymbol{e}^*(\tau)\| \to 0. \tag{94}$$

Since $0 < \eta < k_p$ and relations (93) and (89) hold, one concludes:

$$\exists_{\tau_\gamma > 0} \ : \ \forall_{\tau > \tau_\gamma} \quad \gamma < (k_p - \eta)/(k_p + \eta) \tag{95}$$

and the norm $\| \boldsymbol{e}^*(\tau)\|$ converges asymptotically (exponentially for $\tau > \tau_\gamma$) to zero as $\tau \to \infty$.

In the rest of the proof we consider the convergence of the robot orientation angle φ (called the orientation variable) to the reference angle $\varphi_t \overset{(69)}{=} 0$, at least at the limit $\| \boldsymbol{e}^* \| \to 0$. Due to (89), to show the convergence of φ to zero it suffices to show the convergence to zero for φ_d (Eq. (77)). According to definition (77) it suffices to show, that component h_3 always tends to zero faster, than component h_2 [19]. Recalling (82) and (83) we have for $\varphi_t = 0$:

$$h_2 \overset{\Delta}{=} k_p e_2 - \eta \| \boldsymbol{e}^* \| \, sgn(e_{20}), \qquad h_3 \overset{\Delta}{=} k_p e_3. \tag{96}$$

Moreover, it is easy to show, that (see Appendix):

$$\lim_{\varphi \to \varphi_d} \begin{cases} \dot{x} = h_2, \\ \dot{y} = h_3. \end{cases} \overset{(90)}{\Rightarrow} \lim_{\varphi \to \varphi_d} \begin{cases} \dot{e}_2 = -h_2, \\ \dot{e}_3 = -h_3. \end{cases} \tag{97}$$

Substituting (96) into the above right hand side relations one obtains:

$$\lim_{\varphi \to \varphi_d} \begin{cases} \dot{e}_2 + k_p e_2 &= \eta \| \boldsymbol{e}^* \| \, sgn(e_{20}), \\ \dot{e}_3 + k_p e_3 &= 0. \end{cases}$$

It is obvious, that e_3 tends to zero faster, than e_2. Taking into account (96) it is also clear, that at the limit $\| \boldsymbol{e}^* \| \to 0$ the component $h_3 \to 0$ always faster than h_2. Finally, one concludes:

$$\lim_{\| \boldsymbol{e}^* \| \to 0} \varphi_d(\boldsymbol{e}^*) \to 0 \overset{(89)}{\Rightarrow} \lim_{\tau \to \infty} \varphi(\tau) = 0 \overset{(69)}{\Rightarrow} \lim_{\tau \to \infty} e_1(\tau) = 0.$$

If $\forall_{\tau < \infty} \| \boldsymbol{h}^*(\tau) \| \neq 0$, the term $\dot{\varphi}_d \in \mathcal{L}_\infty$. Now, since h_2, h_3, φ and $\dot{\varphi} \in \mathcal{L}_\infty$, control signals (81) and (87) are bounded and $\lim_{\tau \to \infty} u_1(\tau), u_2(\tau) = 0$. □

Remark 6 *Fulfilling $\| \boldsymbol{h}^* \| \neq 0$ during transient stage depends on the effectiveness of the orienting process – the shorter time interval τ_γ in (95), the earlier convergence of $\boldsymbol{e}^*$ becomes exponential (the norm $\| \boldsymbol{h}^* \|$ will not cross zero in finite time). Hence to guarantee that $\forall_{\tau < \infty} \| \boldsymbol{h}^* \| \neq 0$, the following sequential strategy can be applied:* **S1)** *use the orienting control (81) together with $u_2 \equiv 0$ to fulfill condition (94),* **S2)** *use the complete VFO stabilizer given by Eqs. (81) and (87) ensuring exponential convergence of $\| \boldsymbol{e}^* \|$ to zero.*

Due to (82), the definition (77) is not determined, when the controlled vehicle is at the reference point $\boldsymbol{q}_t^*$, what means $h_2 = h_3 = 0 \;\Rightarrow\; e_2 = e_3 = 0$. Hence, the point $\boldsymbol{e} = \boldsymbol{0}$ is not an equilibrium of the closed loop system, and the proposed VFO controller can be called only as the *almost stabilizer* (according to terminology introduced in [3]). It is worth noticing, that the indeterminacy of the type $\varphi_d = \mathrm{Atan2}\,(0,0)$ never occurs if the condition (95) is met, because assuming $\| \boldsymbol{e}^*(0) \| \neq 0$, it would only occur at the limit $\tau \to \infty$, what theoretically means never [3, 1]. Although from a practical point of view and in the case when $\| \boldsymbol{e}^*(0) \| = 0$, it is desirable to introduce additional definitions of signals φ_d and $\dot{\varphi}_d$ at the origin. As a consequence, one introduces the following proposition of a discontinuous (piecewise continuous) asymptotic stabilizer well defined in the whole error space.

Proposition 5 (VFO stabilizer) *For the given reference point (69), the VFO controller (81) and (87) globally asymptotically stabilizes the point $\boldsymbol{e} = \boldsymbol{0}$ if:*

$$\varphi_d, \dot{\varphi}_d \overset{\Delta}{=} \begin{cases} (77), (80) & for \quad \boldsymbol{e}^* \neq \boldsymbol{0}, \\ \varphi_t, \dot{\varphi}_t & for \quad \boldsymbol{e}^* = \boldsymbol{0}. \end{cases} \tag{98}$$

4 Control limitations

In practice, limitations of the control signals always exist. Hence, not all control values are feasible in a real system. Therefore, in this section the control signals saturation will be explicitly taken into account and robustness of considered stabilization controllers to these saturations will be examined. Now, we define limitations imposed on inputs of the controlled kinematics (1).

Although in Eq. (1) it is assumed, that inputs to the system are, respectively, angular, $u_1 = \Omega$, and linear, $u_2 = V$, velocities of the robot platform, in practice and in the case of differentially driven vehicle, one can physically affect only the configuration velocities, which are left, ω_L, and right, ω_R, robot angular wheel velocities. Since both wheels simultaneously affect signals Ω and V, one cannot independently impose constant limitations Ω_{max} and V_{max} on these inputs (they are related as $\Omega_{max} = f(V_{max})$). Therefore, one has to define limitations concerning configuration velocities ω_L and ω_R. Let us assume, that both wheels and their drives are identical, with r denoting the wheel radius and b denoting the length of the wheel axle (see Fig. 1). Parameter $\omega_{max} > 0$ is the maximal feasible angular velocity of each wheel. The well known linear relation between inputs from and respective configuration velocities is as follows:

$$\boldsymbol{u} = \boldsymbol{\Phi}\,\boldsymbol{\omega}, \tag{99}$$

where

$$\boldsymbol{u} \triangleq \begin{bmatrix} u_1 \\ u_2 \end{bmatrix}, \quad \boldsymbol{\Phi} \triangleq \begin{bmatrix} r/b & -r/b \\ r/2 & r/2 \end{bmatrix}, \quad \boldsymbol{\omega} \triangleq \begin{bmatrix} \omega_R \\ \omega_L \end{bmatrix}.$$

Denoting by $\boldsymbol{u}_c = [u_{1c}\ u_{2c}]^T$ the control vector computed (non-saturated) by one of the presented stabilizers, the computed (non-saturated) configuration velocities follow:

$$\boldsymbol{\omega}_c = \boldsymbol{\Phi}^{-1}\,\boldsymbol{u}_c, \tag{100}$$

where $\boldsymbol{\omega}_c = [\omega_{Rc}\ \omega_{Lc}]^T$. According to work [11] (see also [2]), we propose the following scaling procedure, which guarantees fulfilling configuration input limitations: $|\omega_R|, |\omega_L| \leqslant \omega_{max}$ and preserves the same direction of the computed control vector, $\boldsymbol{u}_c$, and the rescaled (and limited) control vector[3] $\boldsymbol{u}_s$:

$$\boldsymbol{u}_s = \boldsymbol{\Phi}\,\boldsymbol{\omega}_s, \tag{101}$$

where $\boldsymbol{u}_s = [u_{1s}\ u_{2s}]^T$, $\boldsymbol{\omega}_s = [\omega_{Rs}\ \omega_{Ls}]^T$ and

$$s \triangleq \max\left\{\frac{|\omega_{Rc}|}{\omega_{max}}, \frac{|\omega_{Lc}|}{\omega_{max}}\right\}, \qquad \boldsymbol{\omega}_s = \begin{cases} \boldsymbol{\omega}_c & \text{if} \quad s \leqslant 1, \\ \frac{1}{s}\boldsymbol{\omega}_c & \text{if} \quad s > 1. \end{cases} \tag{102}$$

Now, rescaled control vector $\boldsymbol{u}_s$ meets the control limitation $\Omega_{max} = f(V_{max})$ directly resulting from the value of ω_{max} and can be applied to system (1). In the next section aforementioned control limitations will be taken into account during simulation tests. Performances of presented controllers for the cases with and without limitations will be examined and compared.

[3] In a sense, that $\boldsymbol{u}_s \,||\, \boldsymbol{u}_c$ or $\boldsymbol{u}_s = a\boldsymbol{u}_c$, where $0 < a \leqslant 1$.

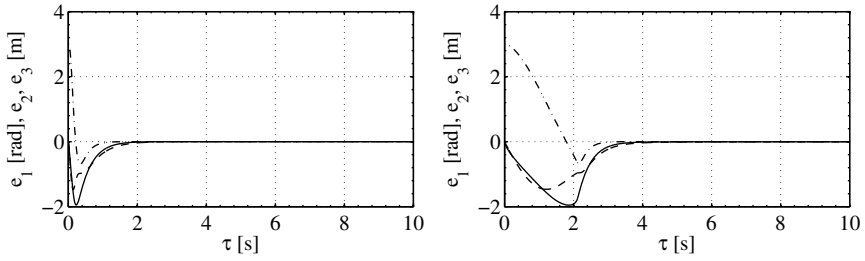

(a) Case A (b) Case B

Figure 4: Posture errors: e_1 (–), e_2 (- -), e_3 (-.-), TVO controller.

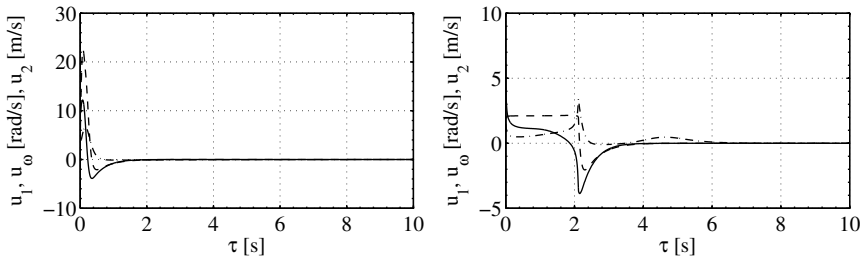

(a) Case A (b) Case B

Figure 5: Control signals: u_1 (–), u_2 (- -) and u_ω (-.-), TVO controller.

5 Simulation results

Effectiveness of both proposed controllers will be illustrated by simulation results. The reference point is located at the origin: $\boldsymbol{q}_t = [0\ 0\ 0]^T$. Numerical simulations have been conducted within the time horizon of $\tau_h = 10[s]$ and for the following initial conditions: $\varphi(0) = 0$, $x(0) = 0$ and $y(0) = -3$ (parallel parking). Both controllers have been tested for two cases: (A) without control signal limitations and (B) when practical limitations of wheel velocities have been imposed. In case (B) the following parameters values have been set[4]: wheel radius: $r = 0.026[m]$, axle length: $b = 0.066[m]$ and maximal wheel velocity: $\omega_{max} = 81[rad/s]$.

5.1 TVO stabilizer

The parameters of the controller presented in Section 3.1.3 have been selected as: $k_1 = k_2 = 6$, $\boldsymbol{\xi}(0) = [0\ \ -1]^T$, $\psi_{10} = \pi$, $\psi_{20} = 4$, $\varepsilon_1 = \varepsilon_2 = 0.01$, $\alpha_1 = 2$ and $\alpha_2 = 3$.

[4]Presented values are the real parameters of the experimental mobile robot *MiniTracker 3* presented in [13].

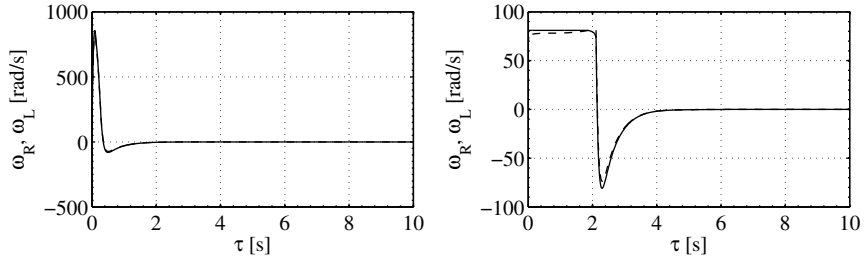

(a) Case A (b) Case B

Figure 6: Robot's wheel velocities: ω_R (–) and ω_L (- -), TVO controller.

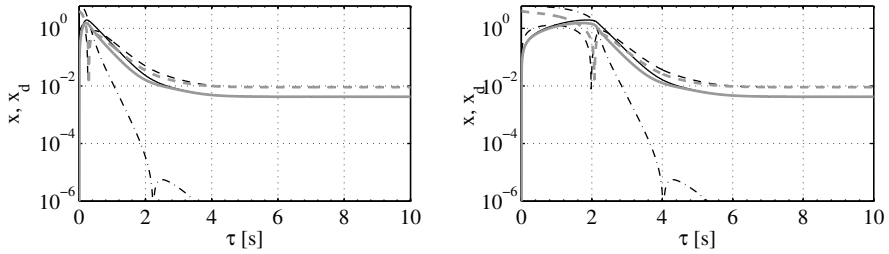

(a) Case A (b) Case B

Figure 7: Auxiliary signals – logarithmic value-scale: (black) x_1 (–), x_2 (- -), x_3 (-.-), (grey) x_{d1} (–), x_{d2} (- -), TVO controller.

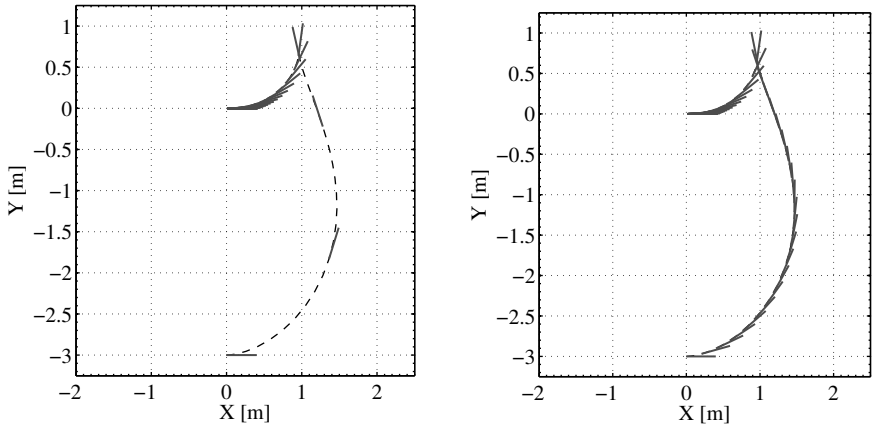

(a) Case A (b) Case B

Figure 8: Robot's path in the task space – parallel parking maneuvers, TVO controller.

5.1.1 Case A.

In Figs. 4(a)-8(a) the results of simulation concerning TVO controller without control saturation are presented. From Fig. 4(a) one can see that errors in Cartesian space converge exponentially to the neighborhood of the origin without significant overshoots. Lack of oscillatory behavior is ensured by making enough high initial value of scaling functions ψ_1 and ψ_2. In Fig. 5(a) control signals: physical, $\boldsymbol{u}$, and virtual, u_ω, are presented. As one can see although initial values of u_ω are quite high, oscillations do not occur since errors decrease fast. In Fig. 7(a) evolution of auxiliary signals $\boldsymbol{x}$ and $\boldsymbol{x}_d$ is depicted. It is interesting to see that vector $\boldsymbol{x}^*$ convergences to $\boldsymbol{x}_d$ while x_3 is driven to zero directly. Therefore, the convergence rate of $\|\boldsymbol{x}\|$ is, in particular, related to convergence rate of ψ_1 and ψ_2 (note that values of gains k_1 and k_2 are chosen to be higher than α_1 and α_2). One can see, that the initial condition of $\boldsymbol{\xi}(0)$ has been chosen such that $x_{d1}(0) = 0$. As a result tracking error with respect to z_1 is quite small from the beginning of regulation process - note that no perfect tracking is related to disturbances by neglecting the term $\dot{\boldsymbol{\Psi}}$ in the control law (compare stability result given by (58)). At the end of regulation errors e_1, e_2 and e_3 are bounded and satisfy inequality (41).

The robot's path in Cartesian space presented in Fig. 8(a) allows to conclude that its shape is quite natural without many hard turns which sometimes appears for control laws using time-varying feedback [3]. The presented strategy allows to avoid oscillatory behavior by proper tuning of the controller and it is not very difficult.

5.1.2 Case B.

In the second simulation experiment control saturations have been included. In order to guarantee stability the algorithm using control signal scaling has been tested. The scaling function μ has been calculated based on formula (102) as follows

$$\mu = \begin{cases} 1 & \text{if} \quad s \leqslant 1, \\ \frac{1}{s} & \text{if} \quad s > 1. \end{cases}$$

Next it has been used to obtain scaled time τ_s according to (62). These variables are depicted in Fig. 9. As one can see at the beginning of regulation process control signals

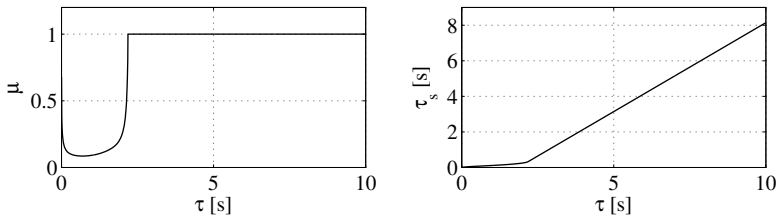

Figure 9: Evolution of scaling function μ (left) and scaled time τ_s (right), TVO controller - **Case B**.

are scaled significantly (about ten times with respect to the original values). After time 2.2[s] signals are not scaled anywhere and the controller behaves as original one. Comparing errors obtained in previous case (see Figs. 4(a), 4(b), 7(a) and 7(b)) one can conclude that presence of saturation makes initial phase of regulation to be slower. However, if error values decrease and the control signal produced by nominal control law remains permissible range then the convergence rate is the same in both cases. It is very interesting to compare the path of the robot. According to Figs. 8(a) and 8(b)

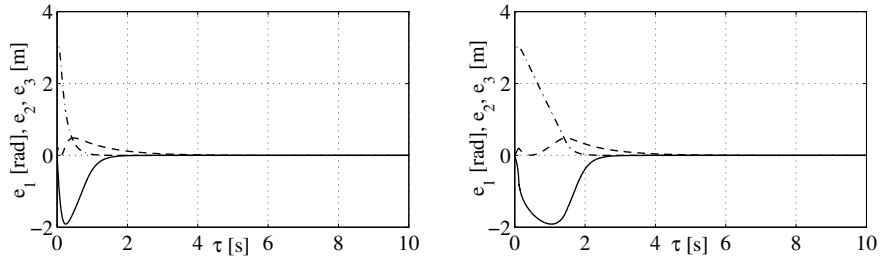

(a) Case A (b) Case B

Figure 10: Posture errors: e_1 (–), e_2 (- -), e_3 (-.-), VFO controller.

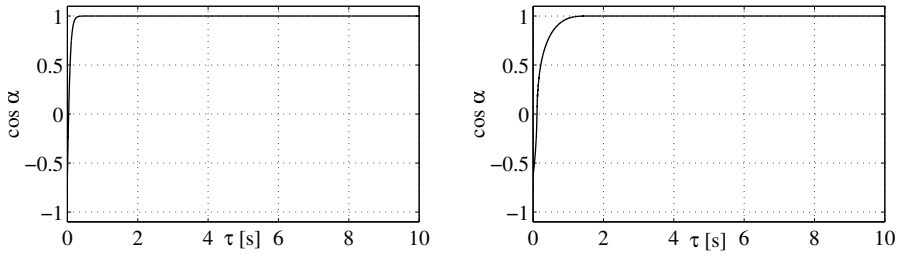

(a) Case A (b) Case B

Figure 11: Time plot of $\cos\alpha$, where $\alpha\angle(\boldsymbol{g}_2^*, \boldsymbol{h}^*)$, VFO controller.

one can see that shapes of trajectories are the same (independent on saturation) which is desirable from a practical point of view.

5.2 VFO controller

During simulations with the VFO controller the set of parameters has been set as follows: $k_1 = 10, k_p = 5$ and $\eta = 4$. Since continuous state variable $\varphi \in \mathbb{R}$ is not limited to the range $[-\pi, \pi)$, to avoid discontinuity in e_{1d} resulting from definition (77), the continuous method of determining the auxiliary variable φ_d has been applied. In the case of unlimited control signals (case (A)), this method can be treated as equivalent to the following formula: $\varphi_d(\tau) = \varphi_d(0) + \int_0^\tau \dot{\varphi}_d(\xi)d\xi$, where $\varphi_d(0)$ is computed by (77), $\dot{\varphi}_d$ is taken from (80) and the integral is computed numerically.

5.2.1 Case A.

Control performance in the case without control signal limitations is presented in Fig. 10(a)-14(a). According to time plots in Fig. 10(a) relative fast error convergence can be seen.

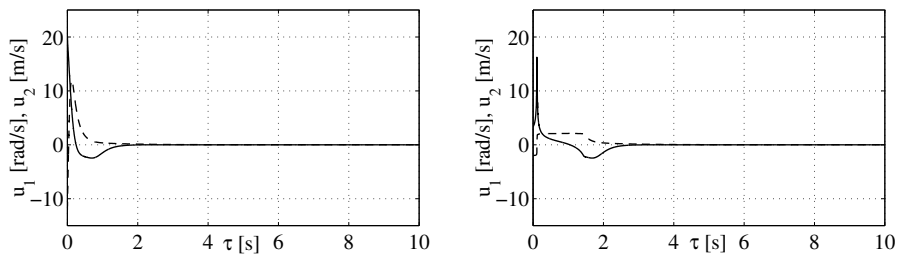

(a) Case A (b) Case B

Figure 12: Control signals: u_1 (–) and u_2 (- -), VFO controller.

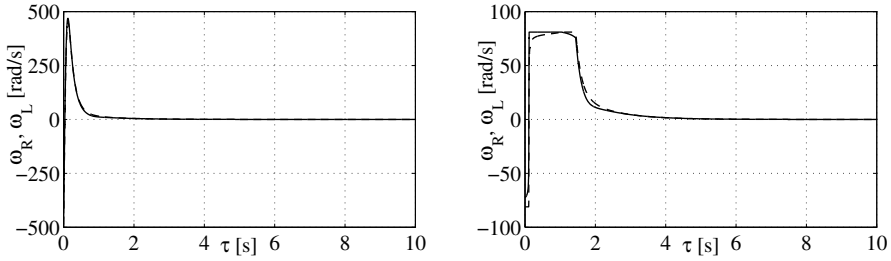

(a) Case A (b) Case B

Figure 13: Robot's wheel velocities: ω_R (–) and ω_L (- -), VFO controller.

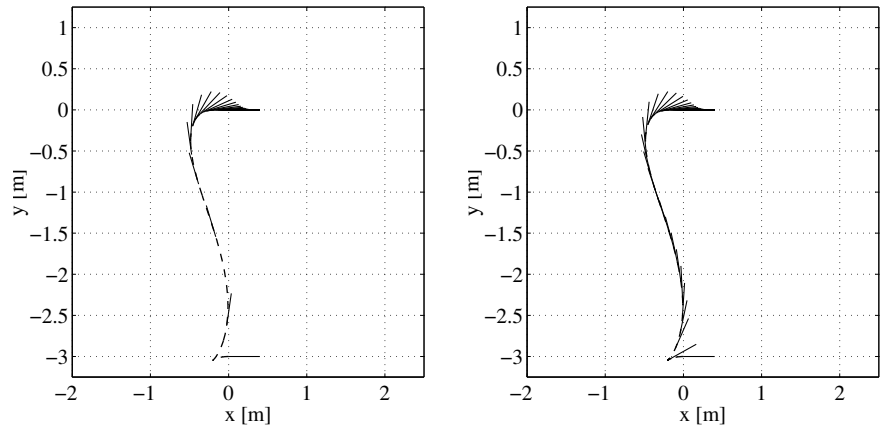

(a) Case A (b) Case B

Figure 14: Robot's path in the task space – parallel parking maneuvers, VFO controller.

The orienting process is very effective since $\cos\alpha \approx +1$ after about $0.5[s]$. It should be noted, that control signals u_1 and u_2 as well as ω_R and ω_L are bounded, non-oscillatory and converge to zero (velocities ω_R and ω_L have been computed using (100), only for comparison purposes with time plots for case B). Figure 14(a) shows the resulted robot path in task space during control process (straight short lines denote instantaneous vehicle orientation). One can find, that the path is quite natural with only one switchback during the transient stage.

5.2.2 Case B.

In this case control signal limitation $\omega_{max} = 81[rad/s]$ has been explicitly specified. *Nominal* equations of the VFO controller (81) and (85) have been followed by the scaling procedure (100)-(102) to limit the computed inputs[5]. Behavior of all signals in this case is presented in Figs. 10(b)-14(b). Error convergence is slower than in case A, but also relatively fast. The orienting process is less effective but $\cos\alpha \approx +1$ after about $1.5[s]$. Comparing Figs. 12(a) and 12(b) it is clear that control signals u_{1s} and u_{2s} are limited and explicit limitation regarding the value of ω_{max} can be observed in Fig. 13(b). It is interesting to note, that resulted vehicle's path shape in task space is preserved in comparison with case A. Only vehicle velocities along the path are rescaled (see different

[5]Note, that terms $\dot{h}_2$ and $\dot{h}_3$ which appear in Eq. (107) are determined also in case B with the *nominal* control $u_2 \equiv u_{2c}$ (not with the rescaled one u_{2s}). Hence, in case B, the feedforward term in definition (81) should be denoted by $\dot{\varphi}_{dc}$ rather than by $\dot{\varphi}_d$. Note also, that in case B: $\dot{\varphi}_{dc} = \Gamma(\tau)\dot{\varphi}_d$, and $\Gamma(\tau) \equiv 1$ if $s \leqslant 1$.

densities of short lines denoting robot orientation in Figs. 14(a) and 14(b)). This feature seems to be very desirable from a practical point of view.

6 Conclusions

In this paper two point-stabilization strategies for a unicycle mobile robot have been presented and numerically tested. The first control strategy comes from the kinematic oscillator and transverse functions concept, which assures practical stability for the cart's posture error. The second control algorithm results from the simple geometrical interpretation and decomposition of a control task into orienting and pushing subtasks. The latter strategy leads to the time invariant discontinuous VFO controller, which guarantees asymptotic posture error convergence to zero. The practical aspect concerning the control signals limitations imposed directly on the vehicle's wheels velocities has been considered. Simulations have been conducted for two cases: without limitations of input signals and with imposed limitations. The control signals scaling procedure has been proposed. Obtained performances have been compared for both cases and both controllers. Future works will be focused on experimental validation of the presented strategies.

Appendix

Derivation of relation (22). Recalling that $\boldsymbol{J}$ is the skew-symmetric matrix, $\boldsymbol{J}^T = -\boldsymbol{J}$, $\boldsymbol{\eta}^T \boldsymbol{J} \boldsymbol{\eta} = 0$, where $\boldsymbol{\eta} \in \mathbb{R}^2$, taking the time derivative of (13) and then using (20) results in

$$\begin{array}{l} \dot{z}_3 = \left(\boldsymbol{x}^{*T} + \boldsymbol{x}_d^T\right) \boldsymbol{J} \boldsymbol{v} + \dot{\boldsymbol{x}}_d^T \boldsymbol{J} \boldsymbol{x}^* = \left(\boldsymbol{x}^{*T} + \boldsymbol{x}_d^T\right) \boldsymbol{J} \left[-k_1 \left(\boldsymbol{x}^* - \boldsymbol{x}_d\right) + \dot{\boldsymbol{x}}_d\right] + \dot{\boldsymbol{x}}_d^T \boldsymbol{J} \boldsymbol{x}^* = \\ = k_1 \left(-\boldsymbol{x}^{*T} \boldsymbol{J} \boldsymbol{x}^* + \boldsymbol{x}_d^T \boldsymbol{J} \boldsymbol{x}_d\right) + k_1 \left(-\boldsymbol{x}_d^T \boldsymbol{J} \boldsymbol{x}^* + \boldsymbol{x}^{*T} \boldsymbol{J} \boldsymbol{x}_d\right) + \\ + \boldsymbol{x}^{*T} \boldsymbol{J} \dot{\boldsymbol{x}}_d + \dot{\boldsymbol{x}}_d \boldsymbol{J} \boldsymbol{x}^* + \boldsymbol{x}_d^T \boldsymbol{J} \dot{\boldsymbol{x}}_d = \boldsymbol{x}_d^T \boldsymbol{J} \dot{\boldsymbol{x}}_d + 2 k_1 \boldsymbol{x}^{*T} \boldsymbol{J} \boldsymbol{x}_d \end{array}$$

Derivation of (56).

Let us assume that positive definite scalar function is written as

$$\dot{V} = -kV + \epsilon \exp\left(-\alpha \tau\right), \tag{103}$$

where $k, \epsilon > 0$ are some scalars. Concerning homogeneous ordinary differential equation $\dot{V} + kV = 0$ one can easily obtain that $V = C \exp\left(-k\tau\right)$, where C denotes some constant. Next using method of variation of parameters one can write that $V = C\left(\tau\right) \exp\left(-k\tau\right)$ and substitute this solution to (103) that yields

$$\dot{C}\left(\tau\right) = \epsilon \exp\left[\left(-\alpha + k\right) \tau\right]. \tag{104}$$

Consequently, integrating the term $\dot{C}\left(\tau\right)$ results in the following solution to (103)

$$V\left(\tau\right) = \begin{cases} V\left(0\right) \exp\left(-k\tau\right) + \dfrac{\epsilon}{k - \alpha} \left[\exp\left(-\alpha\tau\right) - \exp\left(-k\tau\right)\right] & \text{for } \alpha \neq k, \\ V\left(0\right) \exp\left(-k\tau\right) + \epsilon\tau \exp\left(-k\tau\right) & \text{for } \alpha = k. \end{cases} \tag{105}$$

Derivation of (92).

$$\boldsymbol{r} \overset{(91)}{=} \boldsymbol{h}^* - \dot{\boldsymbol{q}}^* \overset{(85)}{=} \| \boldsymbol{h}^* \| \begin{bmatrix} \frac{h_2}{\| \boldsymbol{h}^* \|} - \cos\alpha \cos\varphi \\ \frac{h_3}{\| \boldsymbol{h}^* \|} - \cos\alpha \sin\varphi \end{bmatrix}.$$

Now we can compute (assuming $\| \boldsymbol{h}^* \| \neq 0$):

$$\begin{aligned} \| \boldsymbol{r} \|^2 &= \| \boldsymbol{h}^* \|^2 \left[\tfrac{h_2^2}{\| \boldsymbol{h}^* \|^2} - \tfrac{2h_2 \cos\alpha \cos\varphi}{\| \boldsymbol{h}^* \|} + (\cos\alpha\cos\varphi)^2 + \right. \\ &+ \left. \tfrac{h_3^2}{\| \boldsymbol{h}^* \|^2} - \tfrac{2h_3 \cos\alpha \sin\varphi}{\| \boldsymbol{h}^* \|} + (\cos\alpha\sin\varphi)^2 \right] = \\ &= \| \boldsymbol{h}^* \|^2 \left[1 - 2\cos\alpha \tfrac{h_2\cos\varphi + h_3 \sin\varphi}{\| \boldsymbol{h}^* \|} + \cos^2\alpha \right] = \\ &\overset{(86)}{=} \| \boldsymbol{h}^* \|^2 \left(1 - 2\cos\alpha\cos\alpha + \cos^2\alpha \right) = \| \boldsymbol{h}^* \|^2 \left(1 - \cos^2\alpha \right). \end{aligned}$$

Derivation of (93).

$$\begin{aligned} 1 - \cos^2\alpha &\overset{(86)}{=} 1 - \tfrac{(h_2\cos\varphi + h_3\sin\varphi)^2}{\| \boldsymbol{h}^* \|^2 \left\| \boldsymbol{g}_2^* \right\|^2} = \tfrac{h_2^2 + h_3^2 - (h_2\cos\varphi + h_3\sin\varphi)^2}{h_2^2 + h_3^2} = \\ &= \tfrac{(h_2\sin\varphi - h_3\cos\varphi)^2}{h_2^2 + h_3^2}. \end{aligned}$$

Assuming, that $\varphi \to \varphi_d$ we get $\tan\varphi \overset{(77)}{\to} h_3/h_2$. Using this in the above formula we easily obtain (93).

Derivation of (97).

$$\begin{bmatrix} \dot{x} \\ \dot{y} \end{bmatrix} \overset{(71)}{=} \boldsymbol{g}_2^*(\varphi)\, u_2 \overset{(87)}{=} \begin{bmatrix} \cos\varphi \\ \sin\varphi \end{bmatrix} \boldsymbol{g}_2^{*T} \boldsymbol{h}^* = \begin{bmatrix} h_2\cos^2\varphi + h_3\cos\varphi\sin\varphi \\ h_2\sin\varphi\cos\varphi + h_3\sin^2\varphi \end{bmatrix}.$$

At the limit $\varphi \to \varphi_d$ one gets:

$$\begin{bmatrix} \dot{x} \\ \dot{y} \end{bmatrix} = \begin{bmatrix} h_2\cos^2\varphi_d + h_3\cos\varphi_d\sin\varphi_d \\ h_2\sin\varphi_d\cos\varphi_d + h_3\sin^2\varphi_d \end{bmatrix}, \text{ and} \tag{106}$$

$$\tan\varphi_d \overset{(77)}{=} \frac{h_3}{h_2} \quad \Rightarrow \quad \cos\varphi_d = \frac{h_2\sin\varphi_d}{h_3}, \quad \sin\varphi_d = \frac{h_3\cos\varphi_d}{h_2}.$$

Substituting formulas for $\cos\varphi_d$ and $\sin\varphi_d$ into the appropriate elements in (106) one gets (at the limit $\varphi \to \varphi_d$):

$$\begin{bmatrix} \dot{x} \\ \dot{y} \end{bmatrix} = \begin{bmatrix} h_2\cos^2\varphi_d + h_3\frac{h_2\sin\varphi_d}{h_3}\sin\varphi_d \\ h_2\frac{h_3\cos\varphi_d}{h_2}\cos\varphi_d + h_3\sin^2\varphi_d \end{bmatrix} = \begin{bmatrix} h_2 \\ h_3 \end{bmatrix}.$$

Recalling, that $\dot{e}_2 = -\dot{x}$, $\dot{e}_3 = -\dot{y}$, relation (97) easily follows.

Now components $\dot{h}_2$ and $\dot{h}_3$ which appear in (80) will be described. Recalling the definitions (82) and (83) and assuming (69), simple computations give:

$$\begin{aligned} \dot{h}_2 &= -k_p\dot{x} - \eta\, sgn(e_{20}) \tfrac{x\dot{x} + y\dot{y}}{\sqrt{x^2+y^2}} \overset{(1)}{=} -u_2 \left(k_p\cos\varphi + \eta\, sgn(e_{20}) \tfrac{x\cos\varphi + y\sin\varphi}{\sqrt{x^2+y^2}} \right), \\ \dot{h}_3 &= -k_p\dot{y} \overset{(1)}{=} -u_2(k_p\sin\varphi), \end{aligned} \tag{107}$$

where u_2 is computed by (87).

References

[1] M. Aicardi, G. Casalino, A. Bicchi, and A. Balestrino. Closed loop steering of unicycle-like vehicles via Lyapunov techniques. *IEEE Robotics and Automation Magazine*, 2:27–35, 1995.

[2] G. Artus, P. Morin, and C. Samson. Tracking of an omnidirectional target with a unicycle-like robot: control design and experimental results. Technical Report 4849, INRIA, Sophia Antipolis, France, 2003.

[3] A. Astolfi. *Asymptotic stabilization of nonholonomic systems with discontinuous control*. PhD thesis, Swiss Federal Institute of Technology, Zurich, 1996.

[4] A. M. Bloch. *Nonholonomic mechanics and control*. Systems and Control. Springer, New York, 2003.

[5] R. W. Brockett. Asymptotic stability and feedback stabilization. In R. W. Brockett, R. S. Millman, and H. H. Sussmann, editors, *Differential Geometric Control Theory*, pages 181–191. Birkhäuser, Boston, 1983.

[6] R. W. Brockett, R. S. Millman, and H. J. Sussmann. *Differential Geometric Control Theory*. Birkhäuser, Boston, 1982.

[7] C. Canudas de Wit, H. Khennouf, C. Samson, and O.J. Sørdalen. Nonlinear control design for mobile robots. In Y.F. Zheng, editor, *Recent Trends in Mobile Robots*, volume 11, chapter 5, pages 121–156. World Scientific, Singapore, 1993.

[8] C. Canudas de Wit, B. Siciliano, and G. Bastin. *Theory of Robot Control*. Springer-Verlag, New York, 1996.

[9] W. E. Dixon, D. M. Dawson, E. Zergeroglu, and A. Behal. *Nonlinear control of wheeled mobile robots*. Springer, London, 2001.

[10] I. Dulęba. *Algorithms of motion planning for nonholonomic robots*. Wrocław University of Technology Publishing House, Wrocław, 1998.

[11] P. Dutkiewicz, M. Michalski, and M. Michałek. Robust tracking with control vector constraints. In *Proceedings of the Second International Workshop On Robot Motion and Control*, pages 169–174, Bukowy Dworek, Poland, 2001.

[12] M. Michałek and K. Kozłowski. Control of nonholonomic mobile robot with vector field orientation (in Polish). In K. Tchoń, editor, *Postepy Robotyki*, chapter 4, pages 235–246. Wydawnictwa Komunikacji i Łacznosci, Warsaw, 2005.

[13] T. Jedwabny, M. Kowalski, M. Kiełczewski, M. Ławniczak, M. Michalski, M. Michałek, D. Pazderski, and K. Kozłowski. Nonholonomic mobile robot MiniTracker 3 for research and educational purposes. In *35th International Symposium on Robotics*, 2004.

[14] I. Kolmanovsky and N. H. McClamroch. Developments in nonholonomic control problems. *IEEE Control Systems Magazine*, 15(6):20–36, 1995.

[15] A. De Luca and G. Oriolo. Modeling and control of nonholonomic mechanical systems. In J. Angeles and A. Kecskementhy, editors, *Kinematics and Dynamics of Multi-Body Systems*, chapter 7, pages 277–342. Springer-Verlag, Wien, 1995.

[16] P. Morin and C. Samson. Field oriented control of induction motors by application of the transverse function control approach. In *42nd IEEE Conference on Decision and Control*, pages 5921–5926, 2003.

[17] P. Morin and C. Samson. Practical stabilization of driftless systems on Lie groups: the transverse function approach. *IEEE Transactions on Automatic Control*, 48(9):1496–1508, September 2003.

[18] P. Morin and C. Samson. Trajectory tracking for non-holonomic vehicles: overview and case study. In *Proceedings of the 4th International Workshop On Robot Motion and Control*, pages 139–153, Puszczykowo, 2004.

[19] G. Oriolo, A. De Luca, and M. Vendittelli. WMR control via dynamic feedback linearization: design, implementation and experimental validation. *IEEE Transactions on Control System Technology*, pages 835–852, November 2002.

[20] K. Kozłowski and D. Pazderski. Modelling and control of 4-wheel skid-steering mobile robot. *International Journal of Applied Mathematics and Computer Sciences*, 14(4):477–496, 2004.

[21] D. Pazderski and K. Kozłowski. Practical stabilization of two-wheel mobile robot with velocity limitations using time-varying control law. In *Fith International Workshop on Robot Motion and Control*, pages 205–212, Dymaczewo, Poland, 2005.

[22] C. Samson. Control of chained systems. Application to path following and time-varying point-stabilization of mobile robots. *IEEE Transactions on Automatic Control*, pages 64–77, January 1995.